Innovative Food Science and Emerging Technologies 83 (2023) 103248

Contents lists available at ScienceDirect

Innovative Food Science and Emerging Technologies

journal homepage: www.elsevier.com/locate/ifset

Investigation of novel cold atmospheric plasma sources and their impact on the structural and functional characteristics of pea protein

Fan Bu [a], Samira Feyzi [a], Gaurav Nayak [b], Qingqing Mao [a], V.S. Santosh K. Kondeti [b], Peter Bruggeman [b], Chi Chen [a], Baraem P. Ismail [a,*]

[a] Food Science and Nutrition Department, University of Minnesota, 1334 Eckles Ave, Saint Paul, MN 55108, United States of America
[b] Department of Mechanical Engineering, University of Minnesota, 111 Church St SE, Minneapolis, MN 55455, United States of America

ARTICLE INFO

Keywords:
Cold atmospheric plasma
2D-dielectric barrier discharge
Atmospheric pressure plasma jet
Nanosecond pulsed discharge
Pea protein
Structure and functionality

ABSTRACT

The impact of three cold atmospheric plasma (CAP) sources, atmospheric pressure plasma jet (APPJ), two-dimension dielectric barrier discharge (2D-DBD), and nanosecond pulsed discharge (ns-pulsed) on the structure, functionality, and amino acid composition of pea protein was evaluated. Different plasma sources and associated reactive species resulted in protein denaturation, increased surface hydrophobicity, formation of soluble aggregates mostly by disulfide linkages, and changes in secondary structures. Enhancement in surface properties, presence of soluble aggregates, and increase in β-sheet contributed to significant improvement in gelation and emulsification. Enhanced emulsion stability was attributed to relatively small droplet sizes and high surface-charge. Differences among CAP-treated samples were attributed to differences in fluence and composition of plasma-produced reactive species. While all three plasma treatments could be appreciable functionalization approaches, 2D-DBD ($Ar + O_2$) treatment for 30 min had insignificant effect on the amino acid composition.

Abbreviations used

ATR-FTIR	attenuated total reflectance Fourier transform infrared spectroscopy
APPJ	atmospheric pressure plasma jet
CAP	cold atmospheric plasma
CLSM	confocal laser scanning microscopy
cPPI	commercial pea protein isolate
DSC	differential scanning calorimetry
EC	emulsification capacity
ns-pulsed	nanosecond pulsed discharge
PCA	principal components analysis
PPI	pea protein isolate
RNS	reactive nitrogen species
ROS	reactive oxygen species
SDS-PAGE	sodium dodecyl sulfate-polyacrylamide gel electrophoresis
SE-HPLC	size-exclusion high-performance liquid chromatography
2D-DBD	two- dimension dielectric barrier discharge

1. Introduction

While pea protein is gaining traction in the global plant protein market, its functionality is lagging behind soy protein. In order for pea protein to be successfully in various food application, its functionality needs to be improved by feasible modification approaches. Enzymatic hydrolysis (Arteaga, Guardia, Muranyi, Eisner, & Schweiggert-Weisz, 2020), Maillard-induced glycation (Liu, Ru, & Ding, 2012), and physical modifications (Mirmoghtadaie, Shojaee Aliabadi, & Hosseini, 2016) have been explored to enhance pea protein functionality. However, each of these modifications has limitations including negative impact on flavor, loss of nutritional value, limited industrial feasibility, and/or high energy input and production cost. Additionally, the inherently lower content of the functional, high molecular weight legumin in pea compared to soy, cannot be ameliorated by enzymatic hydrolysis or other traditional physical modifications. Therefore, it is necessary to examine alternative modification approaches, such as cold atmospheric plasma (CAP).

CAP, a novel non-thermal processing technology, has been explored for various applications including pesticide dissipation (Sarangapani et al., 2016), enzyme inactivation (Misra, Pankaj, Segat, & Ishikawa, 2016), water disinfection (Prakash et al., 2017), and microbial inactivation (Moldgy, Nayak, Aboubakr, Goyal, & Bruggeman, 2020). Advantages, including low temperature, and absence of solvents, make CAP a desirable food processing strategy. Plasma, generated by

* Corresponding author.
E-mail address: bismailm@umn.edu (B.P. Ismail).

https://doi.org/10.1016/j.ifset.2022.103248
Received 7 October 2022; Received in revised form 26 November 2022; Accepted 18 December 2022
Available online 21 December 2022

subjecting gases to high voltage, comprises various highly reactive species, such as reactive oxygen species (ROS) (O, O_3, OH, and H_2O_2) and reactive nitrogen species (RNS) (NO_2, HNO_2 and N_2O_5) (Gorbanev, Privat-Maldonado, & Bogaerts, 2018; Moldgy et al., 2020). Different plasma sources produce various reactive species profiles that may induce different chemical reactions including oxidation, polymerization, and bond cleavage. Such reactions can alter the structures of pesticides, enzymes, microbes, and food components such as starch and protein (Surowsky, Bußler, & Schlüter, 2016).

CAP has garnered interest in recent years for its application as a protein modification approach to enhance functionality (Tolouie, Mohammadifar, Ghomi, & Hashemi, 2018). A reduction in sulfhydryl groups coupled with the formation of protein aggregates of high molecular weight (HMW), along with an enhancement in gelation properties of CAP-treated squid proteins was reported by Nyaisaba et al. (2019). Ji et al. (2018) observed an increase in the relative abundance of β-sheet, along with an enhancement in emulsification properties of CAP-treated peanut protein. CAP has also been used to enhance the functionality of pea protein (Bußler, Steins, Ehlbeck, & Schlüter, 2015; Mahdavian Mehr & Koocheki, 2020). Enhancements in solubility of CAP-treated pea protein was observed by Bußler et al. (2015). Improved solubility and emulsion properties of CAP-treated pea protein was also reported by Mahdavian Mehr and Koocheki (2020).

While the reported observations are promising, only remote dielectric barrier discharge (DBD) operating in ambient air has been investigated for pea protein modification in powder form. Various reactive species can be generated by different plasma configurations and gases. Long-lived RNS and ROS (O_3, H_2O_2, NO_2^-, and NO_3^-) dominate in DBD treatment over because the lifetime of short-lived species (OH, singlet oxygen, electrons and ions) is too short to be transported to the protein for remote treatment conditions (Gorbanev et al., 2018). Nonetheless, short-lived species are the main contributors to structural changes of organic compounds (Attri et al., 2016). Additionally, treatment in powder form, in absence of water medium, may limit the variety of the plasma species that can be produced and hinder the efficiency of the plasma species penetration into the sample (Surowsky et al., 2016). Therefore, investigation of other CAP sources to treat pea protein in solution is warranted to provide further information that would be beneficial to guide the use of CAP in the food industry during wet milling and processing.

In our previous study, we observed that OH radicals and O_3, compared to N_xO_y and H_2O_2, had the most significant effect on protein structure and functionality (Bu, Nayak, Bruggeman, Annor, & Ismail, 2022). Thus, plasma treatment modalities that can generate short-lived reactive species and O_3 merit further investigation, while elucidating structural changes as they relate to consequent enhancement in functionality. To achieve this goal, a remote plasma treatment modality mainly delivering O_3 is compared with plasma produced in direct contact with the protein solution, producing a large fluence of a broad range of reactive species including OH, O, singlet oxygen, O_2^-, electrons and positive ions.

For the first time, pea protein in solution was treated with a variety of CAP sources, including direct APPJ coupled with argon (Ar) and O_2, remote DBD coupled with Ar and O_2, and direct nanosecond (ns)-pulsed discharge coupled with air. The overall goal was to investigate the effects of different plasma treatment modalities, as well as treatment time, on pea protein structural and functional changes. This comprehensive work demonstrates the comparative potential of various CAP sources to induce a directed enhancement in pea protein functionality.

2. Materials and methods

2.1. Materials

Yellow field pea flour was supplied by AGT Foods (Regina, SK, Canada), defatted soy flour (7B, 53% protein) by Archer Daniels Midland (ADM) (Decatur, IL, USA), and commercial pea protein isolate (cPPI, 81% protein, 3.9% ash) by Puris Foods (Minneapolis, MN, USA). Laemmli 4× buffer, Tris/Glycine/sodium dodecyl sulfate (SDS) running buffer 10×, Imperial™ Protein Stain, Criterion™ TGX™ 4–20% precast gels, and Precision Plus molecular weight marker were purchased from Bio-Rad Laboratories, Inc. (Hercules, CA, USA). Superdex™ 200 Increase 10/300 GL Prepacked Tricorn™ Column, and HMW and low molecular weight (LMW) calibration kits, were purchased from Cytiva (Marlborough, MA, USA). Sudan Red 7B were purchased from Thermo Fisher Scientific™ (Waltham, MA, USA). Costar® solid opaque black 96-well plates, 8-anilino-1-napthalenesulfonic acid ammonium salt (ANS), dansyl chloride (DC), d5-tryptophan, sulfadimethoxine, and amino acid standards were purchased from Sigma-Aldrich (St. Louis, MO, USA).

2.2. Pea protein isolate (PPI) preparation

PPI was produced as optimized by Hansen (2020) and reported by Bu et al. (2022), following alkaline solubilization at pH 7.5 coupled with isoelectric precipitation at 4.5. The Dumas method (AOAC 990.03), with a conversion factor of 6.25, was used to determine the protein purity of PPI (89.8%), using a LECO® FP828 nitrogen analyzer (LECO, St. Joseph, MI, USA).

2.3. Atmospheric pressure plasma jet (APPJ) treatment

A radio frequency (RF) driven APPJ, as shown in Fig. S1, and described by Kondeti, Zheng, Luan, Oehrlein, and Bruggeman (2020) was used to treat PPI. Briefly, a 2 mm (ID) × 3 mm (OD) cylindrical quartz tube surrounded a 1 mm (ϕ) tungsten needle electrode. A 20 kHz modulated RF signal (13.1 MHz) with a duty cycle of 20% was generated by a function generator (Tektronix AFG 2021), amplified by an RF amplifier (Amplifier Research AF75A250A), and applied through a matching box to the tungsten needle electrode. Argon, at a flow rate of 1.5 standard liters per minute (slm), flowed through the quartz tube and acted as a feed gas for generating the plasma. Oxygen, at a flow rate of 2 slm, flowed through a 12.7 mm (ID) x 19 mm (OD) shielding tube and acted as a shielding gas for preventing the formation of RNS. A 72 mm × 55 mm 100 mL glass beaker containing 50 mL of protein solution (5% *w/v* protein in DDW) was placed on a magnetic stir plate and at a distance of 10 mm below the APPJ nozzle. The dissipated power when the plasma was in contact with the surface of the protein solution was 6.7 ± 1.8 W. Protein solutions, in triplicates, were subjected to plasma treatment for 5, 15, 30, and 45 min, with constant stirring at 200 rpm. The temperature of the solution after treatment ranged between 28 and 30 °C. The Ar plasma jet interacting with the liquid is an abundant source of OH, ions and electrons that in the presence of O_2 can be augmented with O, singlet oxygen and O_3 (Taghvaei, Kondeti, & Bruggeman, 2019).

2.4. Remote two-dimensional dielectric barrier discharge (2D-DBD) treatment

The flow-through plasma reactor as detailed by Nayak, Aboubakr, Goyal, and Bruggeman (2018) and Bu et al. (2022) was used (Fig. S2). The discharge was operated at atmospheric pressure in argon (Ar) with 20% admixture of O_2 (Ultra-Pure-Carrier Grade 99.9993%) with a constant flow rate of 5 slm. The plasma power was kept constant at 10.3 ± 1.1 W in Ar/O_2. Ozon (O_3), was the dominant long-lived species, produced by Ar/O_2 plasma. The O_3 density ($(1.4 \pm 0.2) \times 10^{22}$ m^{-3}) in the Ar/O_2 plasma was measured at 253.4 nm (Nayak, Sousa, & Bruggeman, 2017). A protein solution (100 mL, 5% *w/v* protein in DDW) in a bubbler (PYREX® 500 mL Gas Washing Bottle with Coarse Fritted Cylinder), was subjected to the effluent confined within a polycarbonate tube for treatment time of 5, 15, 30, and 45 min, in triplicate. The temperature of the solution after treatment ranged between 24 and 26 °C. The gas residence time in the effluent of the plasma till it reached the protein solution was ~12 s, which is sufficiently long for all short-

lived reactive species such as O and singlet oxygen to recombine before reaching the protein solution (Nayak et al., 2017). The remote plasma treatment will typically lead to a smaller influx of reactive species in the liquid and a lower rate of liquid phase oxidation reactions compared to the two other direct plasma treatment modalities used in this work (Taghvaei et al., 2019).

2.5. Nanosecond-pulsed (ns-pulsed) plasma treatment

The schematic for the ns-pulsed discharge reactor is shown in Fig. S3a. The setup consisted of a hollow stainless-steel tube with merlon-shaped edge (¼ inch diameter) as the high voltage electrode, which was placed 7.5 mm above a protein solution (100 mL, 5% *w/v* protein in DDW). The solution was grounded to a resistor of 77 Ω to avoid shorting of the high voltage power supply. A ns-pulse generator (NPG-18/3500 N) and surrounding atmospheric air were used to generate a discharge between the powered electrode and the surface of the protein solution by applying voltage pulses at a repetition rate of 1 kHz and an amplitude of ~10 kV. The applied voltage and current in the circuit were recorded using a high-voltage probe (Tektronix P6015A) and a Rogowski coil (Pearson 2877) (Fig. S3a). The phase shift between the voltage and current probes was corrected using the relation between the capacitive current and voltage as measured for voltage pulses that did not lead to plasma formation. The energy in the discharge was determined as the product of the voltage and current waveforms. Protein samples were treated with a fixed pulse energy of ~4 mJ, for 5, 15, and 30 min, in triplicate. The temperature of the solution after treatment ranged between 28 and 30 °C. Due to the high voltage power, 45 min treatment was not possible. The power and the energy deposited on the protein solution as a function of time for a single voltage pulse is shown in Fig. S3b. The positive voltage pulses lead to strong surface discharge at the solution interface enabling the formation of OH radicals.

2.6. Handling of plasma-treated protein solutions

To evaluate the impact of the aforementioned plasma sources on structure and functionality of PPI, lyophilized PPI was dissolved in DDW at 5% protein (*w/v*) and adjusted to pH 2, in triplicate, prior to all plasma treatments. pH 2 was chosen for CAP treatment based on our earlier findings (Bu et al., 2022). Immediately after treatment, the pH of the solutions was adjusted back to pH 7, followed by dialysis using a 3.5 kDa cut-off membrane, lyophilization, and storage at 4 °C. The dialysis step was to ensure the removal of residual salts including long-lived plasma species. The protein (~90%) and ash content (2.5–4.2%) of the lyophilized samples were determined by the Dumas method and the 942.05 AOAC dry ashing method, respectively.

2.7. Color measurement

A Chroma Meter CR-221 (Minolta Camera Co., Osaka, Japan) was used to evaluate, in triplicate, the color of the reference cPPI, control PPI, and CAP-treated samples, as described by Bu et al. (2022). Total color difference (ΔE) between the control PPI and CAP-treated sample was calculated, to determine the impact of the various plasma sources and treatment time on color.

2.8. Protein profiling by gel electrophoresis

SDS polyacrylamide gel electrophoresis (SDS-PAGE) was used for protein profiling of cPPI, control PPI, and all CAP-treated samples following the procedure outlined by Boyle, Hansen, Hinnenkamp, and Ismail (2018). A 4–20% gel was used to load the samples (50 μg protein in 5 μL) and 10 μL MW markers. The gel was then stained, destained, and imaged as reported earlier (Boyle et al., 2018).

2.9. Molecular weight distribution by size-exclusion – High-performance liquid chromatography (SE-HPLC)

Reference cPPI, control PPI, and CAP-treated samples were analyzed by SE-HPLC using a Shimadzu HPLC system (Shimadzu scientific instruments, Colombia, MD, USA) and a Superdex column as outlined by Bruckner-Guhmann, Heiden-Hecht, Sozer, and Drusch (2018) and modified by Bu et al. (2022). In triplicate, 1% protein (*w/v*) samples were prepared in three different buffers, pH 7 phosphate buffer (0.05 M sodium phosphate with 0.1 M sodium chloride), SDS phosphate buffer (0.05 M sodium phosphate with 0.1 M NaCl and 0.1% SDS), and SDS/BME buffer (0.05 M sodium phosphate with 0.1 M NaCl, 0.1% SDS and 2.5% BME) to investigate the molecular weight distribution, degree of polymerization, and association of proteins through covalent and non-covalent interactions. Analysis and detection were performed as described by Bu et al. (2022)

2.10. Differential scanning calorimetry (DSC)

A DSC instrument (DSC 1 STARe System, Mettler Toledo, Columbus, OH, USA) was used to determine the denaturation temperature and enthalpy of the different protein samples (Boyle et al., 2018). Thermograms were integrated using Mettler Toledo's STARe Software (version 11.00).

2.11. Attenuated total reflectance Fourier-transform infrared spectroscopy (ATR-FTIR)

ATR-FTIR spectra of reference cPPI, control PPI, and CAP-treated samples were obtained using Fourier-transform infrared spectrometer (Thermofisher Nicolett iS50 FTIR), as described previously (Bu et al., 2022). OMNIC® software and PeakFit v. 4.12 were used to convert spectra into transmission spectra and to determine the second derivative of Amide *I* band (1600 cm^{-1} -1700 cm^{-1}) for the identification of α-helix, β-sheet, β-turn, and random coil distribution, respectively.

2.12. Measurement of protein surface properties

Surface hydrophobicity of the different samples was determined fluorometrically using ANS probe (Boyle et al., 2018), and modified by Bu et al. (2022). A dynamic light scattering instrument (Malvern Nano *Z*-S Zetasizer) was used to measure zeta potential (Bu et al., 2022). Smoluchowski model, using the Malvern's Zetasizer software (version 7.13), was followed to obtain the zeta potential.

2.13. Protein solubility

Protein solubility at 5% protein (*w/v* in DDW at pH 7) was determined, in triplicate, at room temperature and post thermal treatment (80 °C for 30 min) following the method described by Wang and Ismail (2012) and modified by Bu et al. (2022).

2.14. Gel strength

Heat-induced gel strength at 15% and 20% protein (w/v, in DDW at pH 7), in triplicate, was determined as described by Boyle et al. (2018) and modified by Bu et al. (2022). A TA-TX Plus Texture Analyzer (Stable Micro Systems LTD, Surrey, UK) equipped with a 100 mm diameter probe was used to measure gel strength at 5 mm/s test speed, and a target distance of 0.5 mm from the plate. The maximum force (N) measured was recorded as the rupture force of the gel.

2.15. Emulsification capacity

Emulsification capacity (EC) at 1% and 2% protein (w/v, in DDW at pH 7), in triplicate, was determined following the methods outlined by

Boyle et al. (2018) and modified by Bu et al. (2022). Emulsification capacity was expressed as g of oil emulsified by one g of protein.

2.16. Emulsion physical stability

Emulsions using cPPI, PPI control, and select plasma treated PPI samples with superior EC and hydrophobicity were prepared, in duplicate, at pH 7 and at 2% protein with corn oil, as described by (Hinnenkamp & Ismail, 2021), with modifications. A coarse emulsion was formed by adding corn oil (10% *w/v*) to the protein solution followed by homogenization with a Scilogex D500 probe homogenizer at 10,000 rpm for 1 min (Scilogex, LLC, Rocky Hill, CT). A fine emulsion was formed by passing the coarse emulsion through a 2-stage Panda homogenizer (GEA Niro Soavi North America, Bedford, NH) four times at 300/50 bar. The physical properties of the emulsions were tested immediately and over a 10-day period at two-days intervals. Zeta potential, turbidity, and oil droplet size were determined to characterize the physical properties and stability of the emulsions stored at 40 °C, following the methods described previously (Hinnenkamp & Ismail, 2021). Confocal laser scanning microscopy (CLSM) was used to visualize the microstructure of the fine emulsions at days 0 and 10. For imaging, 1 mL of the fine emulsion was mixed with 15 μL of the Fast Green (10 mg/mL in DDW) and Nile Red (1 mg/mL in methanol), for protein and fat staining, respectively. Approximately 40 μL of the stained emulsion was placed into a walled slide, covered with a coverslip, and equilibrated for 15 min at room temperature before imaging. Image collection was done using a Nikon A1si (NIKON, Champigny sur Marne, France) CLSM with a 60 × (NA 1.40) oil immersion objective lens, at excitation wavelength of 633 and 543 nm for Fast Green and Nile Red, respectively.

2.17. Amino acid and non-protein molecules analysis

To characterize the potential influence of CAP on individual amino acids, control PPI and selected plasma treated PPI samples were analyzed for amino acid compositional changes. Sample selection for this analysis was based on the uniqueness in protein structure and functionality as a result of APPJ, 2D-DBD, and ns-pulsed treatment. Control PPI and plasma treated samples, in triplicate, were hydrolyzed by hydrochloric acid (Mao, 2019). Briefly, 50 mg of sample was mixed with 7 mL of 6 N hydrochloric acid and hydrolyzed at 165 °C for 15 min using a Discover SP-D microwave digester (CEM Corporation, Matthews, NC). After the hydrolysis, 50 μL of hydrolyte was dried by nitrogen and then reconstituted in 500 μL of 50% aqueous acetonitrile. Intact protein samples, in triplicates, were extracted for their small-molecule content, and both the hydrolytes and the PPI extracts were derivatized with dansyl chloride. The derivatized samples were analyzed by ultra-performance liquid chromatography (Acuity HPLC, Waters, Milford, MA, USA) coupled with mass spectrometry (Synapt G2-Si, Waters, Milford, MA, USA) and a BEH C18 UPLC column, following the method described by Wang et al. (2018) and Ma et al. (2019). Characteristics of amino acid composition and non-protein molecules were captured by MarkerLynx software (Waters, Milford, MA, USA) and incorporated into a multivariate data matrix after centroiding, deisotoping, filtering, peak recognition, and integration, as described by Mao et al. (2021), with modifications. The contribution of samples to the principal components was described in a scores scatter plot of a multivariate model. The IPL-responsive metabolites were identified by analyzing the ions contributing to the principal components in a loadings scatter plot. To quantify amino acids, the ratio between the peak area of each amino acid to that of the internal standard was fitted with a standard curve using QuanLynx software (Waters, Milford, MA, USA).

2.18. Statistical analysis

SigmaPlot software version 14.0 for windows (Systat Software, San Jose, CA) was used for to conduct one-way analysis of variance (ANOVA). To determine significant differences ($P \leq 0.05$) among at least three means ($n = 3$), Tukey-Kramer multiple means comparison test was used. To determine significant difference ($P \leq 0.05$) between the means of two samples ($n = 3$), a student's unpaired *t*-test was used.

3. Results and discussion

3.1. Effect of different plasma treatments on PPI color

While minimal changes were noted in lightness (L*), a significant decrease in yellow color (b*) of PPI was observed after all three CAP treatments (Table S1). Bu et al. (2022) reported a similar decrease in b* of PPI upon treatment with OH radicals and O_3. APPJ and ns-pulsed delivered both O_3 and OH among other short-lived reactive species including charged species to the protein solution, while remote DBD only delivered O_3. Therefore, the decrease in b*of PPI after DBD treatment was only attributed to the O_3, whereas the decrease in b* of PPI after APPJ and ns-pulsed treatments could have been attributed to both OH and O_3, as well as other short-lived species. With the greatest number of species at high intensity, ns-pulsed treatment had the greatest effect on color, more so at longer treatment time. A decrease in yellowness is an overall positive effect on the appearance of PPI.

3.2. Effect of different plasma treatments on the protein profile and molecular weight distribution

Under non-reducing conditions, intense smearing and dark bands at the top of the gel indicated the presence of HMW polymerized proteins in reference cPPI (Fig. 1, lane 2, 15, 28). The smearing was less intense, under reducing conditions, yet distinct bands of high intensity remained at the top of the gel, indicating that covalent linkages other than disulfide bonds contributed to the formation of HMW aggregates in cPPI (Fig. 1, lane 8, 21, 33). This high degree of polymerization in cPPI could be detrimental to its functional attributes.

Compared to the control, all plasma treatments (APPJ, 2D-DBD, and ns-pulsed) resulted in protein polymerization, as implied by the observed smearing in the upper region of the gel under non-reducing conditions, coupled with reduced intensities of the legumin, vicilin, and convicilin bands (Fig. 1 a, b, & c). The smearing was absent while the intensities of the legumin, vicilin, and convicilin bands were comparable to those in the control PPI, under reducing conditions. This observation indicated that the polymerization induced by all plasma treatments occurred mostly through disulfide linkages. Protein polymerization was most intense in the ns-pulsed treated samples, followed by APPJ and 2D-DBD samples. The oxidation by O_3, and by OH radicals and other short-lived species, which were present at the highest intensity in ns-pulsed plasma, contributed to the observed polymerization. Protein polymerization through disulfide linkages has been observed previously as a result of remote DBD with air (Mahdavian Mehr & Koocheki, 2020; Meinlschmidt et al., 2016; Nyaisaba et al., 2019). Formation of HMW proteins may enhance functional properties of pea protein, namely gelation and emulsification.

Interestingly, formation of low molecular weight (LMW) peptides (<15 kDa) was observed in APPJ-15 and 30 min samples (Fig. 1a, lanes 5, 6, 11, & 12), as well as ns-pulsed 5–30 min samples (Fig. 1c, lanes 30–32 & 35–37), indicating bond cleavage that was not apparent in 2D-DBD samples (Fig. 1b). Similarly, peptide bond cleavage was not observed in previous reports on remote DBD treatment of proteins. In addition, no bond cleavage was observed after OH radical treatment of pea protein (Bu et al., 2022). Therefore, the newly observed formation of LMW peptides were most likely due to the presence of electrons or other radicals in APPJ and ns-pulsed plasma. Formation of LMW proteins could potentially affect the functionality of pea protein.

SE-HPLC analysis was performed to further characterize the molecular weight distribution of soluble aggregates, functional proteins (legumin, vicilin, and convicilin), and LMW proteins/peptides (Table 1

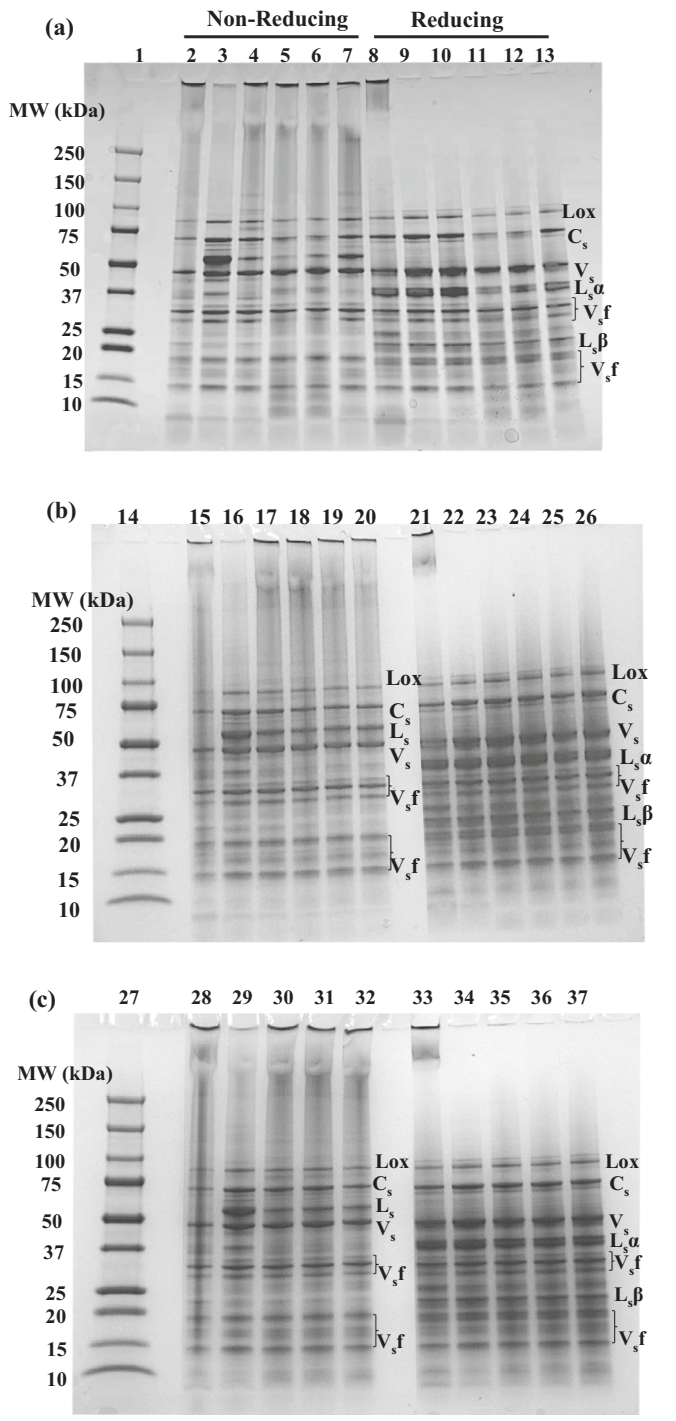

Fig. 1. SDS-PAGE gel visualization of the protein profiles of (a) APPJ treated samples, (b) 2D-DBD treated samples, and (c) ns-pulsed treated samples under non-reducing (Lanes 4-7, 17-20, & 30-32) and reducing (Lanes 10-13, 23-26, & 35-37) conditions. Lanes 1, 14, 27: Molecular weight (MW) marker; Lanes 2, 8, 15, 21, 28, & 33: cPPI; Lanes 3, 9, 16, 22, 29, & 34: control PPI; Lanes 4 & 10, Lanes 5 & 11, Lanes 6 & 12, Lanes 7 & 13: APPJ-5, -15, -30, and -45min, respectively; Lanes 17 & 23, Lanes 18 & 24, Lanes 19 & 25, and Lanes 20 & 26: 2D-DBD-5, -15, -30, and -45min, respectively; Lanes 30 & 35, Lanes 31 & 36, Lanes 32 & 37: ns-pulsed-5, -15, and -30, respectively. Lox: lipoxygenase; C_s: subunits of convicilin; V_s: subunits of vicilin; $L_s\alpha$: acidic peptides cleaved from legumin subunits; $L_s\beta$: basic peptide cleavage from legumin subunit; V_sf: fractions of vicilin subunits result from post-translational cleavages.

and Fig. S4). When samples were prepared in phosphate buffer without SDS or a reducing agent, neither disulfide nor non-covalent bonds among the protein subunits were disrupted. The MW of soluble aggregates was ~1200 kDa, whereas those of hexameric legumin, trimeric convicilin, and trimeric vicilin were within the expected MW ranges (Barac et al., 2010; Gatehouse, Lycett, Croy, & Boulter, 1982; Tzitzikas, Vincken, De Groot, Gruppen, & Visser, 2006). Presumably, insoluble aggregates did not pass through the filter (0.45 μm) and consequently were not seen. The abundance of soluble aggregates and of functional proteins was low in cPPI, indicating that most functional proteins formed insoluble aggregates. Compared to the control PPI, all plasma treated PPIs contained a significantly higher abundance of soluble aggregates. APPJ treatment for 15 and 30 min resulted in a significantly lower relative abundance of soluble aggregates than 45 min treatment. This observation could be in part attributed to bond cleavage after 15 and 30 of APPJ treatment, as shown by SDS-PAGE (Fig. 1a, lanes 5, 6, 11 & 12). The relative abundance of soluble aggregates in 2D-DBD treated PPI was significantly higher after 15 and 30 min of treatment compared to 5 and 45 min. The decrease in soluble aggregates after 45 min 2D-DBD treatment was possibly due to formation of insoluble aggregates. Similarly, the abundance of soluble aggregates decreased significantly in ns-pulsed samples with longer treatment time, indicating the formation of insoluble aggregates, as well. Ji et al. (2018) and Ji et al. (2019) reported an increase in water holding capacity and solubility of peanut protein after short-time DBD (air) treatment, and a decrease in these functional properties after long-time DBD (air) treatment. Our results indicated that the reported decrease in functionality could have been due to the formation of insoluble aggregates.

When SDS was present in the sample buffer, insoluble aggregates formed by non-covalent interactions were solubilized and resulted in a significantly ($P < 0.05$) higher content of soluble aggregates in cPPI and control PPI (Table 1, Fig. S4). The slight decrease in the relative abundance of soluble aggregates in most plasma treated PPIs in the presence of SDS, indicated that few of the interactions within the soluble aggregates were non-covalent. Simultaneously, proteins associating through non-covalent interactions, such as functional proteins, dissociated into subunits with molecular weights <100 kDa (Fig. S4).

When both SDS and BME were present in the sample buffer, insoluble aggregates formed through disulfide linkages and non-covalent interactions were solubilized, and protein subunits linked via disulfide linkages were cleaved into LMW monomers. Reduction of disulfide linkages contributed to the other observed changes in the relative abundance of the different protein fractions (Table 1). Observations were a combined effect of breakdown of insoluble aggregates into soluble aggregates, and reduction of soluble aggregates into monomers. Specifically, the significant increase in the relative abundance of soluble aggregates in 30 min ns-pulsed samples in BME compared to that in SDS, indicated that some insoluble aggregates were formed through disulfide linkages with the longer treatment. Therefore, longer treatment time with an intense plasma source such as ns-pulsed, might not be favorable for protein functionality.

3.3. Effect of different plasma treatments on the protein denaturation state

The two endothermic peaks of vicilin and legumin were observed in the control PPI (Table 2). Convicilin was not seen as a separate endothermic peak because of its structural similarity to vicilin. No endothermic peaks were observed for the reference cPPI, thereby confirming complete denaturation. This observation could be attributing to severe extraction and processing conditions during the production of cPPI, leading to denaturation and consequent polymerization (Fig. 1).

Protein denaturation after remote DBD and APPJ treatment has been reported (Ekezie, Cheng, & Sun, 2019; Meinlschmidt et al., 2016; Sharifian, Soltanizadeh, & Abbaszadeh, 2019). However, there is no report that differentiated the effects of various plasma sources on

Table 1
Molecular weight and relative abundance of soluble aggregates, legumin, convicilin, and vicilin present in commercial pea protein reference (cPPI), control pea protein isolate (PPI), and APPJ, 2D-DBD, ns-pulsed treated PPI samples, as analyzed by size-exclusion high-performance liquid chromatography (SE-HPLC).

Samples	Relative abundance (%) of protein fractions[1]											
	Phosphate buffer[2]				Phosphate buffer (0.1% SDS)[3]				Phosphate buffer (0.1% SDS+ 2.5% BME)[4]			
	Soluble aggregates (~1200 kDa)	Legumin (~450 kDa)	Conviclin (~250 kDa)	Vicilin (~160 kDa)	Soluble aggregates	Legumin	Conviclin	Vicilin	Soluble aggregates	Legumin	Conviclin	Vicilin
cPPI	13.1$^{6cD\delta}$	*[5]	*	3.42$^{bcB\beta}$	45.5$^{aA\alpha}$	*	*	7.30$^{aA\alpha}$	37.3$^{aA\alpha}$	*	*	4.92$^{aA\alpha}$
PPI	4.86$^{dE\varepsilon}$	28.2$^{aA\alpha}$	7.04$^{aA\alpha}$	9.82$^{aA\alpha}$	27.2$^{cC\gamma}$	9.43$^{aA\alpha}$	11.36$^{aA\alpha}$	4.04$^{bB\beta}$	30.0$^{cB\gamma}$	6.58$^{aA\alpha}$	8.72$^{aA\alpha}$	2.77$^{bB\beta}$
APPJ-5 min	26.1^{ab}	4.53^{b}	5.00^{b}	2.83^{c}	24.5^{cd}	4.01^{b}	4.33^{b}	2.14^{c}	27.9^{d}	3.08^{b}	2.55^{b}	1.45^{c}
APPJ-15 min	25.5^{b}	2.29^{c}	4.38^{c}	3.79^{b}	24.^{6cd}	4.31^{b}	3.82^{b}	2.18^{c}	25.2^{e}	2.26^{c}	2.37^{c}	1.02^{e}
APPJ-30 min	25.3^{b}	2.41^{c}	4.08^{c}	3.50^{bc}	22.8^{d}	4.38^{b}	3.62^{b}	1.08^{e}	24.4^{e}	2.11^{d}	2.22^{d}	0.97^{e}
APPJ-45 min	26.9^{a}	3.42^{bc}	4.31^{c}	3.11^{bc}	30.2^{b}	4.87^{b}	2.56^{c}	1.74^{d}	32.6^{b}	2.08^{d}	1.67^{e}	1.23^{d}
2D-DBD-5 min	22.6^{C}	5.14^{B}	5.19^{B}	2.57^{C}	23.8^{D}	4.29^{B}	4.37^{B}	2.22^{C}	22.8^{C}	3.15^{B}	2.75^{BC}	1.56^{C}
2D-DBD-15 min	29.4^{B}	4.19^{D}	4.32^{C}	2.00^{CD}	21.2^{D}	4.35^{B}	4.49^{B}	2.12^{C}	18.4^{D}	2.86^{C}	2.58^{CD}	1.31^{D}
2D-DBD-30 min	34.7^{A}	3.91^{E}	4.15^{C}	1.57^{D}	32.8^{B}	3.52^{B}	3.72^{B}	1.65^{D}	29.5^{B}	2.53^{D}	2.52^{D}	1.17^{DE}
2D-DBD-45 min	24.9^{C}	4.50^{C}	4.90^{B}	1.66^{D}	24.0^{D}	4.17^{B}	4.53^{B}	1.68^{D}	18.2^{D}	2.70^{CD}	2.83^{B}	1.08^{E}
ns-pulsed-5 min	36.7$^{\alpha}$	5.08$^{\beta}$	5.88$^{\beta}$	3.01$^{\beta}$	32.1$^{\beta}$	5.02$^{\beta}$	5.75$^{\beta}$	2.81$^{\Upsilon}$	32.5$^{\beta}$	3.75$^{\Upsilon}$	3.61$^{\beta}$	1.66$^{\Upsilon}$
ns-pulsed-15 min	32.7$^{\beta}$	5.42$^{\beta}$	5.95$^{\beta}$	2.95$^{\beta}$	29.0$^{\beta\Upsilon}$	5.33$^{\beta}$	5.80$^{\beta}$	2.69$^{\Upsilon}$	29.6$^{\Upsilon}$	4.21$^{\beta}$	3.51$^{\beta}$	2.16$^{\beta\Upsilon}$
ns-pulsed-30 min	27.4$^{\Upsilon}$	3.69$^{\beta}$	3.69$^{\Upsilon}$	3.01$^{\beta}$	21.6$^{\delta}$	3.56$^{\beta}$	3.74$^{\Upsilon}$	2.90$^{\Upsilon}$	25.5$^{\delta}$	2.62$^{\delta}$	2.05$^{\Upsilon}$	1.59$^{\Upsilon}$

[1] Relative abundance (%) is the area of a specific peak divided by the total peak area for that sample.
[2] Samples were dissolved in pH 7 phosphate buffer and analyzed by high-performance size exclusion chromatography (SE-HPLC).
[3] Samples were dissolved in pH 7 phosphate buffer with the presence of 0.1% SDS and analyzed by high-performance size exclusion chromatography (SE-HPLC).
[4] Samples were dissolved in pH 7 phosphate buffer with the presence of 0.1% SDS and 2.5% BME, and analyzed by high-performance size exclusion chromatography (SE-HPLC).
[5] An asterisk (*) represents no peak was apparent in this molecular weight range.
[6] Means ($n = 3$) in each column with lowercase letters indicate significant differences of APPJ samples in comparison to nPPI and cPPI, upper letters indicate significant differences of 2D-DBD samples in comparison to nPPI and cPPI, and Greek alphabet indicate significant differences of ns-pulsed samples in comparison to nPPI and cPPI, according to the Tukey-Kramer multiple means comparison test ($P < 0.05$).

protein denaturation. In this study, all plasma treated PPI had a significantly lower denaturation temperature and enthalpy compared to the control PPI (Table 2). The extent of protein denaturation, as indicated by the enthalpy, was greater with longer plasma treatment time, regardless of the plasma sources. Among all plasma treated samples, the 30 min ns-pulsed treated PPI had the lowest enthalpy for vicilin. The presence of intense long-lived and shorted lived reactive species in ns-pulsed plasma contributed to this observation. Protein unfolding can facilitate polymerization, as more hydrophobic residues and sulfhydryl groups are exposed. The higher extent of denaturation in the 30 min ns-pulsed treated PPI resulted in the higher level of observed polymerization in this sample. Bu et al. (2022) reported that both OH and O_3 species resulted in similar denaturation pattern. APPJ treatment, which produced OH and O_3 species, reduced the enthalpy to a greater extent than DBD treatment did, which only generated long-lived O_3.

3.4. Effect of different plasma treatments on the protein surface properties

Surface hydrophobicity significantly increased after APPJ treatment, and with longer exposure time (Table 2). The greater extent of protein denaturation with the increase in APPJ treatment time (5–45 min) contributed to the noted increase in surface hydrophobicity. While 2D-DBD treatment for 5 min did not result in a significant increase in surface hydrophobicity, increasing treatment time from 5 to 15 and 30 min did. Increases in surface hydrophobicity affect protein interactions and consequently their functional properties.

The surface hydrophobicity of the 45 min 2D-DBD sample was significantly lower than that of other 2D-DBD samples. The observed decrease in the relative abundance of soluble aggregates after 45 min of 2D-DBD treatment compared to shorter treatment times (Table 1), coupled with the higher degree of denaturation (Table 2) and reduced surface hydrophobicity, confirmed that the formation of insoluble aggregates was in part due to hydrophobic interactions. Similarly, the surface hydrophobicity of the 30 min ns-pulsed treated sample was significantly lower than that of the 5 and 15 min ns-pulsed treated samples, thus explaining the observed decrease in the relative abundance of soluble aggregates and the formation of polymers through hydrophobic interactions.

Surface charge can also directly affect protein functionality. Owing to changes in the conformation and relative exposure of different groups, protein denaturation and polymerization can affect surface charge. The reference cPPI had the least net surface charge (Table 2), mostly attributed to the high content of insoluble aggregates. Compared to the control, no significant differences in surface charge were noted after APPJ treatment. The net surface charge after 15–45 min of 2D-DBD treatment, and after ns-pulsed treatment (all times) was significantly lower than that of the control. This observed decrease in surface charge was in part due to the extent of denaturation and polymerization.

Table 2
Denaturation temperatures and enthalpy, secondary structure, surface hydrophobicity and surface charge of commercial pea protein reference (cPPI), control pea protein isolate (PPI), and APPJ, 2D-DBD, and ns-pulsed treated PPI.

Samples	Denaturation temperature and enthalpy				Surface properties		Secondary structure			
	Vicilin		Legumin		Surface hydrophobicity	Surface charge	α Helix	β Sheet	β Turn	Random coil
	Denaturation Temperature (Td, °C)	Enthalpy of denaturation (ΔH, J g-1)	Denaturation Temperature (Td, °C)	Enthalpy of denaturation (ΔH, J g-1)	RFI	mV	%			
cPPI	*[1]	*	*	*	$12719^{a\alpha}$	$-27.2^{aA\alpha}$	$14.5^{cB\beta}$	$46.3^{aBC\alpha\beta}$	$24.8^{aA\alpha}$	$14.5^{aA\alpha}$
PPI	$84.48^{aA\alpha}$	$6.39^{aA\alpha}$	91.36^{a}	1.48^{a}	$8545^{dBC\beta}$	-37.6^{bD}	$23.3^{aA\alpha}$	$44.9^{abC\beta}$	$22.8^{aA\alpha}$	$9.02^{bBC\beta\gamma}$
APPJ-5 min	81.65^{b}	1.66^{b}	90.40^{a}	0.20^{b}	9349^{bc}	-37.3^{b}	19.9^{ab}	43.7^{a}	22.1^{a}	14.3^{a}
APPJ-15 min	82.56^{ab}	1.35^{bc}	*	*	10774^{abc}	-35.4^{b}	18.9^{abc}	45.5^{a}	20.6^{a}	15.0^{a}
APPJ-30 min	82.00^{b}	0.97^{cd}	*	*	10146^{bc}	-35.1^{b}	17.4^{bc}	44.7^{a}	21.3^{a}	16.5^{a}
APPJ-45 min	81.56^{b}	0.76^{d}	*	*	11459^{ab}	-36.5^{b}	20.6^{ab}	42.2^{b}	22.1^{a}	15.1^{a}
2D-DBD-5 min	82.49^{B}	1.72^{B}	*	*	8526^{BC}	-36.2^{CD}	14.8^{B}	49.7^{A}	26.1^{A}	9.40^{BC}
2D-DBD-15 min	82.01^{BC}	1.34^{BC}	*	*	9203^{BC}	-34.9^{BC}	17.3^{B}	48.3^{AB}	25.8^{A}	8.65^{BC}
2D-DBD-30 min	80.92^{D}	1.15^{C}	*	*	10415^{B}	-34.5^{BC}	17.0^{B}	49.9^{A}	25.6^{A}	7.56^{C}
2D-DBD-45 min	81.72^{C}	1.25^{C}	*	*	8500^{C}	-33.5^{B}	17.0^{B}	46.0^{BC}	26.3^{A}	10.7^{B}
ns-pulsed-5 min	81.56^{β}	1.77^{δ}	*	*	12088^{α}	-34.4^{β}	16.6^{β}	47.4^{α}	28.3^{α}	7.68^{γ}
ns-pulsed-15 min	81.74^{β}	1.49^{γ}	*	*	12354^{α}	-34.4^{β}	15.9^{β}	48.3^{α}	24.4^{α}	9.57^{β}
ns-pulsed-30 min	82.05^{β}	0.48^{β}	*	*	9580^{β}	-36.1^{β}	16.3^{β}	48.6^{α}	24.6^{α}	10.6^{β}

[1] An asterisk (*) represents no peak of denaturation observed; Means (n = 3) in each column with lowercase letters indicate significant differences of APPJ samples in comparison to nPPI and cPPI, upper letters indicate significant differences of 2D-DBD samples in comparison to nPPI and cPPI, and Greek alphabet indicate significant differences of ns-pulsed samples in comparison to nPPI and cPPI, according to the Tukey-Kramer multiple means comparison test ($P < 0.05$).

However, observed differences are considerably minor mostly due to formation of soluble aggregates that retained high net surface charge, and in part due to the production of LMW proteins.

3.5. Effect of plasma treatments on the protein secondary structure

The distribution of secondary structure elements in PPI (Table 2) was similar to that observed by Beck, Knoerzer, and Arcot (2017). The reference cPPI had a significantly lower relative content of α helix and a higher relative amount of random coil compared to the control PPI, indicating that protein denaturation occurred at the secondary structure level. The significant decrease in the relative abundance of α helix was observed after APPJ, 2D-DBD, and ns-pulsed treatment, also indicated protein denaturation at the secondary structure level. With the decrease in the relative amount of α helix, an increase in random coil was observed after APPJ treatment, whereas an increase in β sheet was noted after 2D-DBD and ns-pulsed treatments. Changes in random coil versus β sheet content will have different impacts on protein functionality. For

Table 3
Solubility, gel strength and emulsification capacity of commercial pea protein reference (cPPI), control pea protein isolate (PPI), and APPJ, 2D-DBD, and ns-pulsed treated PPI.

Samples	Solubility (5% protein)		Gel strength (20% protein)	Emulsification capacity (2% protein)	Emulsification capacity (1% protein)
	Non-Heated	Heated (80 °C for 30 min)	Strength (N)	mL oil/g protein	mL oil/g protein
cPPI	$24.7^{2dE\varepsilon}$	$45.5^{cC\beta}$	$2.73^{eD\gamma}$	$229.4^{cD\beta}$	*[1]
PPI	$82.4^{aA\alpha}$	$79.6^{aA\alpha}$	$4.00^{eD\gamma}$	$390.6^{dE\beta}$	*
APPJ-5 min	64.5^{c}	77.2^{ab}	6.25^{d}	582.8^{a}	812.2^{ab}
APPJ-15 min	68.4^{b}	72.3^{b}	12.3^{b}	533.2^{b}	737.8^{b}
APPJ-30 min	68.1^{b}	75.2^{ab}	14.0^{a}	496.0^{b}	762.6^{b}
APPJ-45 min	65.7^{bc}	76.5^{ab}	10.3^{c}	613.8^{a}	886.6^{a}
2D-DBD-5 min	61.7^{C}	74.5^{AB}	13.3^{AB}	536.3^{C}	750.2^{B}
2D-DBD-15 min	49.0^{D}	69.2^{B}	12.5^{B}	582.8^{AB}	762.6^{B}
2D-DBD-30 min	68.3^{B}	78.1^{A}	14.7^{A}	610.7^{A}	837.0^{A}
2D-DBD-45 min	52.1^{D}	71.0^{B}	10.3^{C}	564.2^{BC}	830.8^{A}
ns-pulsed-5 min	72.2^{β}	76.5^{α}	10.4^{β}	585.9^{α}	818.4^{α}
ns-pulsed-15 min	67.3^{γ}	80.3^{α}	8.82^{β}	585.9^{α}	843.2^{α}
ns-pulsed-30 min	61.1^{δ}	80.3^{α}	12.2^{α}	567.3^{α}	756.4^{α}

[1] An asterisk (*) represents no emulsion formed at 1% protein concentration; Means (n = 3) in each column with lowercase letters indicate significant differences of APPJ samples in comparison to PPI and cPPI, upper letters indicate significant differences of 2D-DBD samples in comparison to PPI and cPPI, and Greek alphabet indicate significant differences of ns-pulsed samples in comparison to PPI and cPPI, according to the Tukey-Kramer multiple means comparison test ($P < 0.05$).

example, increases in β sheet structure resulted in enhanced gelling and emulsification properties of various plant and animal proteins (Cao & Mezzenga, 2019).

3.6. Effect of plasma treatments on protein functionality

Protein solubility is essential for beverage applications, and it can influence gelation and emulsification properties, which are important for other food systems. The reference cPPI had the lowest solubility among the samples (Table 3), under both non-heated and heated conditions. This observation was expected due to cPPI's degree of denaturation, high extent of polymerization and content of insoluble aggregates, comparatively high surface hydrophobicity, and low surface charge. Compared to control PPI, a modest and sometimes significant decrease in solubility, under non-heated conditions, was observed after most plasma treatments. Under heated conditions, the solubility of most plasma treated samples was comparable to that of the control. Changes in solubility were minor due mostly to the formation of larger proportion of soluble aggregates relative to insoluble aggregates. Additionally, the enhancement in solubility upon heating of the plasma treated samples indicated that some of the aggregates formed during the treatment were associated by non-covalent interactions, some of which (H-bonding and electrostatic interactions) are disrupted upon heating. In contrast, the solubility of cPPI, while enhanced upon heating, remained relatively low because the insoluble aggregates present in cPPI were mostly formed through disulfide and other covalent linkages (Fig. 1). This observation is promising for non-thermal CAP processing compared to thermal processing employed during the production of cPPI.

The reference cPPI exhibited the lowest gel strength followed by the control PPI (Table 3). The poor gel strength of cPPI was mostly due to its low solubility, high extent of aggregation, and imbalance of surface charge to surface hydrophobicity ratio, whereas the undesirable gel strength of the control PPI was attributed mostly to the intrinsic protein profile that is low in legumin content, and partly to the comparatively low surface hydrophobicity to surface charge ratio. Legumin contains cysteine residues that can form inter- and intra-molecular disulfide linkages, contributing to gel strength. On the other hand, a good surface charge to hydrophobicity balance is essential to facilitate protein-water and protein-protein interactions, and thus contribute to a well-structured gel. All plasma treated PPIs exhibited a significantly higher gel strength compared to the control PPI and to cPPI. This observation can be attributed to the formation of soluble aggregates, the increased surface hydrophobicity, and to the surface charge that remained relatively high after the different plasma treatments. Soluble aggregates (Table 1), as well as the increased surface hydrophobicity (Table 2), facilitated the formation of 3D gel networking, while the relatively high surface charge (Table 2) enabled protein-water interactions. The 30 min 2D-DBD treated sample exhibited significantly higher gel strength compared to most other plasma treated samples. In addition to presence of soluble aggregates and increased surface hydrophobicity, enhanced gelation can be partially attributed to higher β sheet content in the 30 min 2D-DBD treated sample compared to the control PPI. Presence of soluble aggregates and increase in surface hydrophobicity was also observed after APPJ and ns-pulsed treatments, along with relatively higher β sheet content after ns-pulsed treatments, contributing to enhanced gelation. The observed protein cleavage induced by electrons and radicals under different conditions and intensities could have also contributed to gelation. APPJ samples treated for 15 and 30 min had a significantly higher gel strength compared to those treated for 5 and 45 min. The plasma-induced bond cleavages, seen in the 15 and 30 min APPJ samples, could have reduced the size of insoluble aggregates, contributing further to balanced interactions.

The emulsification capacity (EC) was measured at both 1% and 2% protein concentration, since neither the cPPI nor the control PPI formed an emulsion at 1% protein concentration (Table 3). Differences in EC values among plasma treated samples had similar trend at both protein concentrations. The higher EC values at 1% protein concentration were likely due to relatively less protein-protein interactions and more protein-oil and protein-water interactions at the interface. While the reference cPPI and control PPI formed an emulsion at 2% protein concentration, both had the lowest EC among the samples, but for different reasons. Poor EC of cPPI could be attributed to the high content of large insoluble aggregates, poor hydrophilic/lipophilic balance, and limited solubility that hinders protein migration to the interface. Conversely, the poor EC of the control PPI could be attributed to the inherent characteristics of the dominant proteins, compact and inflexible structure (not denatured), and the relatively high surface charge to hydrophobicity ratio. The EC, however, was significantly enhanced after all plasma treatments due to the structural changes that allowed for better protein adsorption at the interface, at both 1% and 2% protein. Denaturation, which contributed to a more flexible protein structure, coupled with enhanced surfaced hydrophobicity, allowed for easier migration to and better adsorption at the interface.

3.7. Effect of plasma treatments on emulsion physical stability

In addition to cPPI and control PPI, three plasma treated samples, APPJ-45 min, 2D-DBD-30 min, ns-pulsed-5 min, were selected for emulsion physical stability evaluations over 10 days of storage, by measuring zeta potential, droplet particle size, and turbidity, and by visualization of emulsion structure using CLSM. These three treated samples were selected based on distinctive structural characteristics and enhanced EC. The zeta potential of all samples at day 0 fell within −35 to −43 mV (Table 4), indicating adequate repulsive forces to limit emulsion flocculation over time (Hunt & Dalgleish, 1995). However, the zeta potential significantly decreased for all samples after 10 days of storage at 40 °C. At both day 0 and day 10, cPPI had significantly the lowest zeta potential. The three plasma treated samples had significantly higher zeta potential than both cPPI and control PPI after 10 days of storage. While the zeta potential for control PPI dropped markedly, that of the treated samples was only moderately reduced. This observation indicated better physical stability of emulsions formed with plasma treated samples.

In general, an increase in turbidity over storage correlates with an increase in flocculation due to reduction in electrostatic repulsion among the oil droplets. Emulsion turbidity is related to interfacial area and particle size (Britten & Giroux, 1991). Compared to the control PPI and other treated samples, 2D-DBD-30 min emulsion had the lowest turbidity with no measured increase after 10 days of storage. It was expected that cPPI emulsion, which had the highest turbidity at day 0, to have a significant increase in turbidity after 10 days of storage. On the contrary, a slight decrease in the turbidity of cPPI emulsion was noted over storage. cPPI had a significant increase in mean droplet size, along with a wide shift in D10-D90 distribution (Table 4, and Fig. 2). Based on theoretic calculations, there is a polynomial correlation between turbidity and emulsion droplet size for samples larger than a tenth of the wavelength of incident light (Zhang & Reineccius, 2016). Thus, turbidity reaches a maximum at a light wavelength close to the particles size, with further increase in particle size resulting in lower turbidity (Gregory, 2005; Hernandez, Baker, & Crandall, 1991). Chantrapornchai, Clydesdale, and McClements (1998) reported that emulsion turbidity (absorbance at 350–750) increases when oil droplet size increases up to 2 or 3 μm, while further increase in droplet size results in lower turbidity.

A profound bimodal droplet size distribution behavior, characterized by two peaks representing small individual droplets and large droplet flocs, was observed for cPPI emulsion at day 10 (Fig. 2i, A). While cPPI showed a marked increase in droplet size over storage, the change for control PPI was more modest (Table 4). The droplet distribution of control PPI emulsion converted to a bimodal droplet size distribution after 10 days of storage, with only a shallow peak with wider droplet size range (Fig. 2i, B). However, the emulsions of plasma treated samples had minimal change in particle size distribution (Table 4) and retained their

Table 4
Assessment of emulsion physical stability by measuring changes in zeta potential, turbidity, and emulsion oil droplet size distribution over storage.

	Zeta potential (mV)		Turbidity @ 485 nm		d[4,3][1] (μm)		D10 – D90[2] (μm)	
Samples	Day 0	Day 10	Day 0	Day 10	Day 0	Day 10	Day 0	Day 10
cPPI	-35.9^{a}	-29.4^{a*}	0.78^{a}	0.73^{b*}	0.453^{a}	8.362^{a*}	0.185^{a} - 0.543^{a}	0.279^{a*} - 11.536^{a*}
PPI	-43.8^{c}	-32.3^{b*}	0.64^{d}	0.74^{a*}	0.330^{c}	0.685^{b*}	0.181^{b} - 0.490^{c}	0.176^{b} - 1.966^{b*}
APPJ-45 min	-40.5^{b}	-37.2^{cd*}	0.68^{b}	0.76^{a*}	0.326^{c}	0.326^{c}	0.181^{b} - 0.490^{c}	0.178^{b} - 0.492^{b}
2D-DBD-30 min	-41.4^{b}	-36.4^{d*}	0.66^{c}	0.65^{c*}	0.356^{c}	0.429^{c*}	0.182^{b} - 0.525^{b}	0.180^{b} - 0.492^{b}
ns-pulsed-5 min	-40.9^{b}	-34.8^{d*}	0.67^{c}	0.75^{a*}	0.438^{b}	0.448^{c}	0.180^{b} - 0.531^{b}	0.178^{b} - 0.511^{b}

[1] d[4,3] values show the mean (n = 3) volume diameter of the droplets.
[2] D10 – D90 values indicate that 10–90% of the emulsion droplets have diameters in presented size range. Lowercase letters indicate significant differences among means ($n = 3$) in each column according to the Tukey means comparison test ($P < 0.05$).
[*] Indicates significant difference between Day 0 and Day 10 values within an emulsion sample as tested by student's unpaired t-test ($P < 0.05$).

unimodal particle size distribution over storage (Fig. 2i, C-E).

Visualization of emulsions microstructures using CLSM complemented above observations. Aggregation of proteins in cPPI emulsion (in green), and flocculation of oil droplets (red) after 10 days of storage were pronounced (Fig. 2ii, B-1). To a milder extent, control PPI emulsion also underwent protein association and non-uniform distribution of oil droplets after 10 days of storage (Fig. 2ii, B-2). Although homogenization produced fine emulsions with small particle size, over time reduced surface charge would allow protein aggregation and flocculation of the oil droplets, which ultimately results in phase separation. The plasma treated samples produced more uniform and stable emulsions over storage (Fig. 2ii, B-3, B-4, B-5), indicating better adsorption of plasma treated pea proteins at the water/oil interface and resistance to aggregation due to higher surface charge. Such behavior could be the result of the partial unfolding and the presence of soluble aggregates that enhanced protein migration and interactions at the water/oil interface (Ji et al., 2019).

3.8. Effect of different plasma treatments on the amino acid profile and non-protein components of the isolates

Amino acid composition is a key factor when considering the nutritional quality of a food product. Takai et al. (2014) reported chemical modifications of free amino acids after CAP treatment. Therefore, it was essential to investigate any potential changes in the amino acid composition of PPI after CAP treatment. A significant decrease in tyrosine was observed after APPJ and ns-pulsed treatments, compared to the control PPI and the 2D-DBD sample treated for 30 min (Table S2). Nitration and hydroxylation of aromatic rings in tyrosine after direct APPJ (He) treatment was reported previously (Takai et al., 2014). Electrons, OH radicals, positive ions among other reactive species were present in the APPJ (He) treatment. Similarly, direct APPJ ($Ar + O_2$) and ns-pulsed (air) treatment in this study produced short-lived reactive species such as electrons and OH radicals, which could have been responsible for the observed reduction in tyrosine. Remote 2D-DBD treatment, on the other hand, without the presence of radicals and electrons, and with potentially low fluence of O_3 had negligible impact on the tyrosine content. Chen et al. (2019) reported similar result, where the amino acid composition of milk proteins was not significantly impacted by the remote DBD treatment. While a decrease in tyrosine was observed after APPJ and ns-pulsed treatment, the overall amino acid composition was not majorly altered by the tested plasma treatments.

Small portion of sugar, fat, color, and flavor compounds were also present in PPI. An untargeted chemometric analysis was, therefore, conducted to investigate plasma-induced changes in non-protein components. The scores plot of a principal components analysis (PCA) model showed that the chemical composition of PPI was significantly altered after plasma treatment (Fig. 3). Two principal components accounted for 60% of the variance in chemical composition of the control and plasma treated PPI samples. The first component (PC1) represented 36% of the variability. PC1 separated the APPJ 5 min, APPJ 30 min, and control PPI samples, indicating that the changes in chemical composition of PPI after APPJ treatment was time dependent. PC2, accounting for 24% of the variability, separated the APPJ, 2D-DBD, ns-pulsed treated samples, and the control, indicating that changes in chemical composition was also related to plasma sources. Structural identification and quantification of the compounds impacted by plasma treatment need further investigation to assess the safety of plasma treated samples.

4. Conclusions

This work established, for the first time, the effect of different CAP sources (APPJ, 2D-DBD, and ns-pulsed) on the color, structure, functionality, and amino acid composition of pea protein. Outcomes of this study provided the basis for further CAP treatment optimization to induce targeted protein functionality enhancement. All three CAP treatments resulted in protein structural changes that contributed to enhanced gelation and emulsification properties of pea protein, while imparting minimal effects on its amino acid composition. Specifically, 2D-DBD ($Ar + O_2$) treatment for 30 min is a comparatively appreciable functionalization approach due to its modest and desirable structural changes, insignificant effect on amino acid composition, and significant enhancement in functionality. APPJ and ns-pulsed treatments, which also delivered favorable functionality enhancements, need further optimization in terms of intensity, gas used, and treatment time. While all three setups can potentially be scaled up for industrial applications, evaluating the feasibility of industrial scaling would be a natural follow up to this work. Finally, further characterization of newly formed compounds after CAP treatment is needed to evaluate the safety of using CAP in protein modification.

Credit authorship contribution statement

Fan Bu - Conceptualization, Methodology, Execution of experiments, Investigation, Formal data analysis, Writing - original draft. Samira Feyzi - Methodology, Execution of experiments, Writing – review. Gaurav Nayak - Methodology, Writing – review. Qingqing Mao - Methodology, Execution of experiments, Writing – review. V.S. Santosh K. Kondeti - Methodology, Writing – review. Peter Bruggeman - Conceptualization, Methodology, Writing – review. Chi Chen - Conceptualization, Methodology, Writing – review. Baraem P. Ismail - Conceptualization, Project management, Writing - review & editing, Funding acquisition.

Declaration of Competing Interest

The authors declare that they have no known competing financial interests or personal relationships that could have appeared to influence the work reported in this paper.

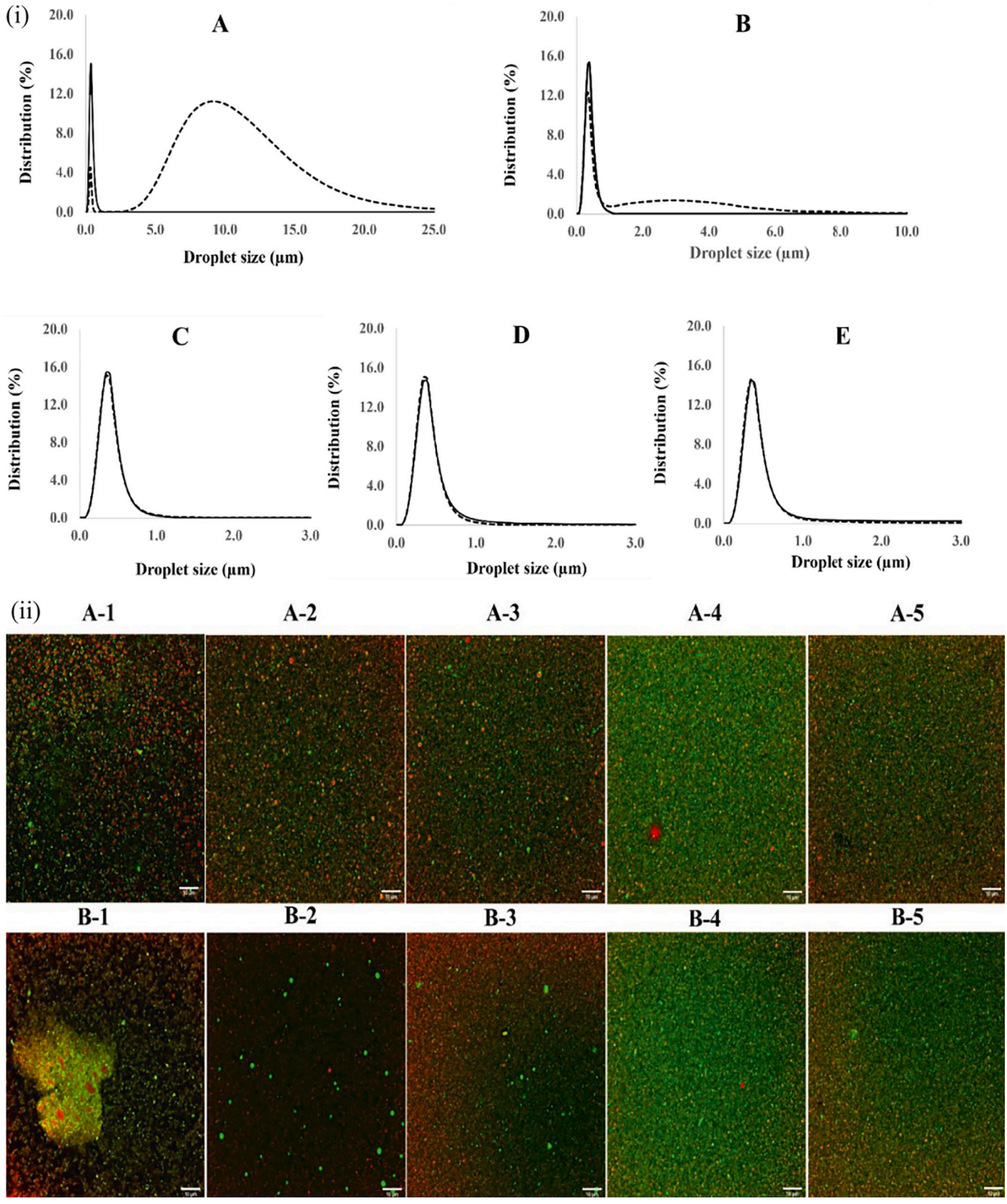

Fig. 2. (i) Changes in droplet distribution over storage for emulsions made with cPPI (A), control PPI (B), APPJ-45min (C), 2D-DBD-30min (D), and ns-pulsed-5min (E). Solid line and dashed line indicate Day 0 and 10, respectively. (ii) Confocal fluorescence micrographs of emulsions stabilized by cPPI (1), control PPI (2), APPJ-45min (3), 2D-DBD-30min (4), and ns-pulsed-5min (5) at day 0 (A) and day 10 (B). White scale bar indicates a length of 10 μm.

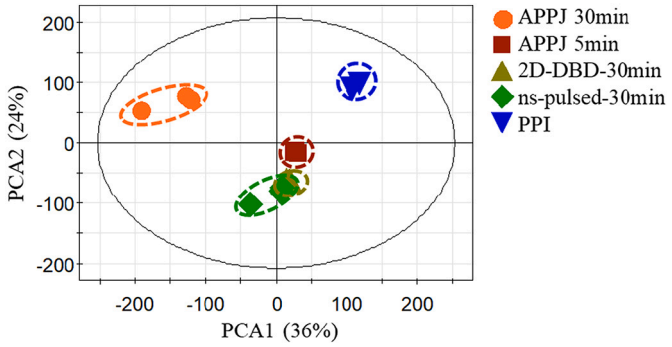

Fig. 3. Scores plot of the principal components analysis (PCA) model produced from the pooled LC-MS analysis of amino acids and non-protein components. The samples in the same treatment group are circled (n=3).

Data availability

Data will be made available on request.

Acknowledgment

This project was funded by the Plant Protein Innovation Center (PPIC). FTIR-ATR data collection was performed at the Characterization Facility, University of Minnesota, which receives partial support from the NSF through the MRSEC (Award Number DMR-2011401) and the NNCI (Award Number ECCS-2025124) programs. CLSM images were captured and analyzed with the support of the resources and staff at the University Imaging Centers (UIC) at University of Minnesota (SCR-020997).

Appendix A. Supplementary data

Supplementary data to this article can be found online at https://doi.org/10.1016/j.ifset.2022.103248.

References

Arteaga, V. G., Guardia, M. A., Muranyi, I., Eisner, P., & Schweiggert-Weisz, U. (2020). Effect of enzymatic hydrolysis on molecular weight distribution, techno-functional properties and sensory perception of pea protein isolates. *Innovative Food Science & Emerging Technologies, 65*, Article 102449.

Attri, P., Yusupov, M., Park, J. H., Lingamdinne, L. P., Koduru, J. R., Shiratani, M., … Bogaerts, A. (2016). Mechanism and comparison of needle-type non-thermal direct and indirect atmospheric pressure plasma jets on the degradation of dyes. *Scientific Reports, 6*(1), 1–14.

Barac, M., Cabrilo, S., Pesic, M., Stanojevic, S., Zilic, S., Macej, O., & Ristic, N. (2010). Profile and functional properties of seed proteins from six pea (*Pisum sativum*) genotypes. *International Journal of Molecular Sciences, 11*(12), 4973–4990. https://doi.org/10.3390/ijms11124973

Beck, S. M., Knoerzer, K., & Arcot, J. (2017). Effect of low moisture extrusion on a pea protein isolate's expansion, solubility, molecular weight distribution and secondary structure as determined by Fourier transform infrared spectroscopy (FTIR). *Journal of Food Engineering, 214*, 166–174. https://doi.org/10.1016/j.jfoodeng.2017.06.037

Boyle, C., Hansen, L., Hinnenkamp, C., & Ismail, B. P. (2018). Emerging camelina protein: Extraction, modification, and structural/functional characterization. *Journal of the American Oil Chemists' Society, 95*(8), 1049–1062.

Britten, M., & Giroux, H. J. (1991). Coalescence index of protein-stabilized emulsions. *Journal of Food Science, 56*(3), 792–795.

Bruckner-Guhmann, M., Heiden-Hecht, T., Sozer, N., & Drusch, S. (2018). Foaming characteristics of oat protein and modification by partial hydrolysis. *European Food Research and Technology, 244*(12), 2095–2106. https://doi.org/10.1007/s00217-018-3118-0. , Dec.

Bu, F., Nayak, G., Bruggeman, P., Annor, G., & Ismail, B. P. (2022). Impact of plasma reactive species on the structure and functionality of pea protein isolate. *Food Chemistry, 371*, Article 131135.

Bußler, S., Steins, V., Ehlbeck, J., & Schlüter, O. (2015). Impact of thermal treatment versus cold atmospheric plasma processing on the techno-functional protein properties from *Pisum sativum* 'Salamanca'. *Journal of Food Engineering, 167*, 166–174.

Cao, Y., & Mezzenga, R. (2019). Food protein amyloid fibrils: Origin, structure, formation, characterization, applications and health implications. *Advances in Colloid and Interface Science, 269*, 334–356.

Chantrapornchai, W., Clydesdale, F., & McClements, D. J. (1998). Influence of droplet size and concentration on the color of oil-in-water emulsions. *Journal of Agricultural and Food Chemistry, 46*(8), 2914–2920.

Chen, D., Peng, P., Zhou, N., Cheng, Y., Min, M., Ma, Y., Mao, Q., Chen, P., Chen, C., & Ruan, R. (2019). Evaluation of *Cronobacter sakazakii* inactivation and physicochemical property changes of non-fat dry milk powder by cold atmospheric plasma. *Food Chemistry, 290*, 270–276.

Ekezie, F.-G. C., Cheng, J.-H., & Sun, D.-W. (2019). Effects of atmospheric pressure plasma jet on the conformation and physicochemical properties of myofibrillar proteins from king prawn (*Litopenaeus vannamei*). *Food Chemistry, 276*, 147–156.

Gatehouse, J. A., Lycett, G. W., Croy, R. R. D., & Boulter, D. (1982). The post-translational proteolysis of the subunits of vicilin from pea (*Pisum sativum L.*). *Biochemical Journal, 207*(3), 629–632. https://doi.org/10.1042/bj2070629

Gorbanev, Y., Privat-Maldonado, A., & Bogaerts, A. (2018). Analysis of short-lived reactive species in plasma–air–water systems: The dos and the do nots. *Analytical Chemistry, 90*(22), 13151–13158. https://doi.org/10.1021/acs.analchem.8b03336

Gregory, J. (2005). *Particles in water: Properties and processes*. CRC Press.

Hansen, L. (2020). *The optimization and scale-up of pea protein extractions and impact on structural and functional properties*.

Hernandez, E., Baker, R., & Crandall, P. (1991). Model for evaluating turbidity in cloudy beverages. *Journal of Food Science, 56*(3), 747–750.

Hinnenkamp, C., & Ismail, B. P. (2021). Enhancing emulsion stability: The synergistic effect of combining Procream and partially hydrolyzed whey protein. *International Dairy Journal, 105059*. https://doi.org/10.1016/j.idairyj.2021.105059

Hunt, J. A., & Dalgleish, D. G. (1995). Heat stability of oil-in-water emulsions containing milk proteins: Effect of ionic strength and pH. *Journal of Food Science, 60*(5), 1120–1123.

Ji, H., Dong, S., Han, F., Li, Y., Chen, G., Li, L., & Chen, Y. (2018). Effects of dielectric barrier discharge (DBD) cold plasma treatment on physicochemical and functional properties of peanut protein. *Food and Bioprocess Technology, 11*(2), 344–354.

Ji, H., Han, F., Peng, S., Yu, J., Li, L., Liu, Y., Chen, Y., Li, S., & Chen, Y. (2019). Behavioral solubilization of peanut protein isolate by atmospheric pressure cold plasma (ACP) treatment. *Food and Bioprocess Technology, 12*(12), 2018–2027.

Kondeti, V. S. K., Zheng, Y., Luan, P., Oehrlein, G. S., & Bruggeman, P. J. (2020). O·, H·, and· OH radical etching probability of polystyrene obtained for a radio frequency driven atmospheric pressure plasma jet. *Journal of Vacuum Science & Technology A: Vacuum, Surfaces, and Films, 38*(3), Article 033012.

Liu, J., Ru, Q., & Ding, Y. (2012). Glycation a promising method for food protein modification: Physicochemical properties and structure, a review. *Food Research International, 49*(1), 170–183. https://doi.org/10.1016/j.foodres.2012.07.034

Ma, Y., Zhou, W., Chen, P., Urriola, P. E., Shurson, G. C., Ruan, R., & Chen, C. (2019). Metabolomic evaluation of scenedesmus sp. as a feed ingredient revealed dose-dependent effects on redox balance, intermediary and microbial metabolism in a mouse model. *Nutrients, 11*(9), 1971.

Mahdavian Mehr, H., & Koocheki, A. (2020). Effect of atmospheric cold plasma on structure, interfacial and emulsifying properties of grass pea (*Lathyrus sativus L.*) protein isolate. *Food Hydrocolloids, 106*, Article 105899. https://doi.org/10.1016/j.foodhyd.2020.105899

Mao, Q. (2019). *Characterizing intense pulsed light-elicited effects on Escherichia coli and non-fat dry Milk through Metabolomic and Chemometric analysis*.

Mao, Q., Liu, J., Wiertzema, J. R., Chen, D., Chen, P., Baumler, D. J., … Chen, C. (2021). Identification of Quinone degradation as a triggering event for intense pulsed light-elicited metabolic changes in *Escherichia coli* by Metabolomic fingerprinting. *Metabolites, 11*(2), 102.

Meinlschmidt, P., Ueberham, E., Lehmann, J., Reineke, K., Schlüter, O., Schweiggert-Weisz, U., & Eisner, P. (2016). The effects of pulsed ultraviolet light, cold atmospheric pressure plasma, and gamma-irradiation on the immunoreactivity of soy protein isolate. *Innovative Food Science & Emerging Technologies, 38*, 374–383.

Mirmoghtadaie, L., Shojaee Aliabadi, S., & Hosseini, S. M. (2016). Recent approaches in physical modification of protein functionality. *Food Chemistry, 199*, 619–627. https://doi.org/10.1016/j.foodchem.2015.12.067

Misra, N., Pankaj, S., Segat, A., & Ishikawa, K. (2016). Cold plasma interactions with enzymes in foods and model systems. *Trends in Food Science & Technology, 55*, 39–47.

Moldgy, A., Nayak, G., Aboubakr, H. A., Goyal, S. M., & Bruggeman, P. J. (2020). Inactivation of virus and bacteria using cold atmospheric pressure air plasmas and the role of reactive nitrogen species. *Journal of Physics D: Applied Physics, 53*(43), Article 434004.

Nayak, G., Aboubakr, H. A., Goyal, S. M., & Bruggeman, P. J. (2018). Reactive species responsible for the inactivation of feline calicivirus by a two-dimensional array of integrated coaxial microhollow dielectric barrier discharges in air. *Plasma Processes and Polymers, 15*(1), 1700119.

Nayak, G., Sousa, J. S., & Bruggeman, P. J. (2017). Singlet delta oxygen production in a 2D micro-discharge array in air: Effect of gas residence time and discharge power. *Journal of Physics D: Applied Physics, 50*(10), Article 105205.

Nyaisaba, B. M., Miao, W., Hatab, S., Siloam, A., Chen, M., & Deng, S. (2019). Effects of cold atmospheric plasma on squid proteases and gel properties of protein concentrate from squid (*Argentinus ilex*) mantle. *Food Chemistry, 291*, 68–76.

Prakash, R., Hossain, A. M., Pal, U., Kumar, N., Khairnar, K., & Mohan, M. K. (2017). Dielectric barrier discharge based mercury-free plasma UV-lamp for efficient water disinfection. *Scientific Reports, 7*(1), 1–8.

Sarangapani, C., Misra, N., Milosavljevic, V., Bourke, P., O'Regan, F., & Cullen, P. (2016). Pesticide degradation in water using atmospheric air cold plasma. *Journal of Water Process Engineering, 9*, 225–232.

Sharifian, A., Soltanizadeh, N., & Abbaszadeh, R. (2019). Effects of dielectric barrier discharge plasma on the physicochemical and functional properties of myofibrillar proteins. *Innovative Food Science & Emerging Technologies, 54*, 1–8.

Surowsky, B., Bußler, S., & Schlüter, O. (2016). Cold plasma interactions with food constituents in liquid and solid food matrices. In *Cold plasma in food and agriculture* (pp. 179–203). Elsevier.

Taghvaei, H., Kondeti, V., & Bruggeman, P. (2019). Decomposition of crystal violet by an atmospheric pressure RF plasma jet: The role of radicals, ozone, near-interfacial reactions and convective transport. *Plasma Chemistry and Plasma Processing, 39*(4), 729–749.

Takai, E., Kitamura, T., Kuwabara, J., Ikawa, S., Yoshizawa, S., Shiraki, K., Kawasaki, H., Arakawa, R., & Kitano, K. (2014). Chemical modification of amino acids by atmospheric-pressure cold plasma in aqueous solution. *Journal of Physics D: Applied Physics, 47*(28), Article 285403.

Tolouie, H., Mohammadifar, M. A., Ghomi, H., & Hashemi, M. (2018). Cold atmospheric plasma manipulation of proteins in food systems. *Critical Reviews in Food Science and Nutrition, 58*(15), 2583–2597. https://doi.org/10.1080/10408398.2017.1335689?needAccess=true

Tzitzikas, E. N., Vincken, J.-P., De Groot, J., Gruppen, H., & Visser, R. G. F. (2006). Genetic variation in pea seed globulin composition. *Journal of Agricultural and Food Chemistry, 54*(2), 425–433. https://doi.org/10.1021/jf0519008

Wang, L., Yao, D., Urriola, P. E., Hanson, A. R., Saqui-Salces, M., Kerr, B. J., … Chen, C. (2018). Identification of activation of tryptophan–NAD+ pathway as a prominent metabolic response to thermally oxidized oil through metabolomics-guided biochemical analysis. *The Journal of Nutritional Biochemistry, 57*, 255–267.

Wang, Q., & Ismail, B. (2012). Effect of Maillard-induced glycosylation on the nutritional quality, solubility, thermal stability and molecular configuration of whey proteinv. *International Dairy Journal, 25*(2), 112–122.

Zhang, J., & Reineccius, G. A. (2016). Factors controlling the turbidity of submicron emulsions stabilized by food biopolymers and natural surfactant. *LWT- Food Science and Technology, 71*, 162–168.